Intrinsic flow and tearing mode rotation in the RFP during improved confinement ⒻF

D. Craig ⒾD, E. H. Tan ⒾD, B. Schott, J. K. Anderson ⒾD, J. Boguski, D. J. Den Hartog, T. Nishizawa ⒾD, M. D. Nornberg ⒾD, and Z. A. Xing

COLLECTIONS

Ⓕ This paper was selected as Featured

View Online   Export Citation   CrossMark

ARTICLES YOU MAY BE INTERESTED IN

Spectroscopic technique sheds insights on how confined plasmas flow
Scilight **2019**, 300007 (2019); https://doi.org/10.1063/1.5119247

Influence of 3D plasmoid dynamics on the transition from collisional to kinetic reconnection
Physics of Plasmas **26**, 072121 (2019); https://doi.org/10.1063/1.5100737

Unified modeling of both resonant and non-resonant neoclassical transport under non-axisymmetric magnetic perturbations in tokamaks
Physics of Plasmas **26**, 072504 (2019); https://doi.org/10.1063/1.5099376

Intrinsic flow and tearing mode rotation in the RFP during improved confinement

D. Craig,[1,a] E. H. Tan,[1] B. Schott,[1] J. K. Anderson,[2] J. Boguski,[2] D. J. Den Hartog,[2] T. Nishizawa,[2]
M. D. Nornberg,[2] and Z. A. Xing[2]

AFFILIATIONS

[1]Department of Physics, Wheaton College, Wheaton, Illinois 60187, USA
[2]Department of Physics, University of Wisconsin-Madison, Madison, Wisconsin 53706, USA

[a]Electronic mail: darren.craig@wheaton.edu

ABSTRACT

We use charge exchange recombination spectroscopy to make the first localized measurements of impurity ion flow velocity profiles in the reversed field pinch. Measurements in improved confinement plasmas reveal an intrinsic flow profile that is peaked on the axis and mostly parallel to the equilibrium magnetic field. The toroidal flow decreases in time at off-axis locations where tearing modes are resonant, giving rise to a highly sheared flow profile near the axis. The tearing mode phase velocity correlates strongly with toroidal flow near the resonant surface and weakly with flow in other locations, providing an opportunity to verify the commonly held assumption that the plasma and mode move together at the resonant surface. Mechanisms for the observed momentum loss during the improved confinement period are evaluated, and it is found that eddy currents in the conducting shell caused by the rotation of the dominant tearing mode dominate over other losses.

Published under license by AIP Publishing. https://doi.org/10.1063/1.5095620

I. INTRODUCTION

Intrinsic plasma flows, those fluid motions naturally arising in confined plasmas without external momentum input, have received much attention recently because of their importance for the success of future devices like ITER.[1,2] These flows are driven by fluctuation-induced stresses and are often associated with the transport of other quantities like particles and energy.[3] Nearly all toroidal plasma systems rotate spontaneously to some degree. Reversed field pinch (RFP) plasmas exhibit intrinsic flows in both the poloidal and toroidal directions.

Much previous work has been done to measure and understand the plasma flows in the RFP. Passive Doppler spectroscopy has been used in a number of devices to measure impurity ion flows in both the core and the edge.[4–9] Insertable probes of various kinds have also been used to measure ion flows and the associated radial electric fields in the edge.[10–13] The intrinsic toroidal flows in large present-day devices can be significant ($\sim$0–60 km/s) and are always in the cocurrent direction in the core. The toroidal flow in the edge (which is mostly perpendicular to B in the edge of the RFP) is generally opposite in direction to the flow in the core. The poloidal flows are smaller than the toroidal ones ($\sim$0–10 km/s) and also commonly exhibit a sign reversal between the core and the edge.

One of the motivations for studying flows in the RFP has historically been the strong connection between the rotation of large scale magnetic fluctuations and the plasma flow. In fact, the motion of resonant tearing modes has often been used to infer the motion of the plasma, assuming that the modes move with the plasma near the mode resonant surface.[13–17] Intrinsic flow drive mechanisms cause the plasma and modes to rotate spontaneously in the lab frame, and the Maxwell and Reynolds stresses produced by the modes also act back on the flow profile.[13,18] The relaxation of the current profile that is mediated by the modes is accompanied by forces that modify the flow profile as well.[13,19] Interaction of the modes with surrounding conducting walls and with magnetic field errors can also have a strong effect on the plasma rotation in the RFP.[17,20–22] These effects are interesting scientifically but are also important to understand on a practical level. For example, the locking of the modes to the wall and the associated increase in plasma-wall interaction has often been an important limitation on RFP operation.[23,24] The relative motion of modes and plasma and the prevention of mode locking are also very important in tokamaks.[25–27]

Measurements of the "kinetic stress" in the Madison Symmetric Torus[28] (MST) recently provided strong evidence that much of the intrinsic flow in the core of the RFP may be the result of this mechanism.[29] The kinetic stress arises due to a correlation between fluctuations in plasma pressure and magnetic field. During times where the fluctuations are suppressed by inductive current profile control,[30] the

kinetic and other stresses that drive intrinsic rotation in standard RFP plasmas are significantly reduced in the core. Recent measurements in the edge of these plasmas revealed new high frequency fluctuations and zonal flows in the region where the steepest density and temperature gradients exist.[31] Previous measurements of flow profiles in these Pulsed Parallel Current Drive (PPCD) plasmas have been limited to the extreme edge due to diagnostic limitations.

In this paper, we describe the first localized flow profile measurements by charge exchange recombination spectroscopy (CHERS) in a reversed field pinch. A diagnostic neutral beam[32] and custom high-throughput spectrometer[33] are used to make fast time-resolved measurements of carbon flows during periods of improved confinement in MST. The CHERS system on MST has been used in the past to measure impurity ion temperature,[34,35] impurity ion densities,[36] and ion velocity fluctuations associated with the tearing modes.[37] Recent improvements in absolute wavelength calibration have enabled equilibrium impurity ion flow profile measurements for the first time.

Our measurements show that the ion flow in MST is primarily parallel to the mean magnetic field in the core and is peaked on the axis. As PPCD proceeds and the plasma confinement improves, the toroidal flow in much of the plasma gradually slows, coincident with a slowing of the dominant tearing mode rotation and consistent with a lack of substantial intrinsic flow drive. However, a small region near the magnetic axis does not slow down, resulting in the development of a strongly sheared flow profile near the axis. We directly examine the connection between tearing mode rotation and ion flows in these discharges and find that the mode rotation is strongly correlated with the ion flow at the resonant surface and weakly correlated with the flow away from the resonant surface. Somewhat surprisingly, the mode rotation is much better correlated with the toroidal flow than with the poloidal flow which is largely unaffected during the slowing down of the modes and toroidal flow. We evaluate various potential mechanisms for the observed momentum loss during PPCD and conclude that the best explanation is a drag on the plasma produced by eddy currents in the conducting shell which are generated by the rotation of the dominant tearing mode.

The presentation of these results is organized as follows: in Sec. II, we describe the experimental setup and diagnostics used. In Sec. III, we describe the method used for absolute wavelength calibration of the spectrometer which enabled these measurements for the first time. Section IV describes the flow profile measurements in PPCD plasmas with CHERS and places them in context relative to other measurements of flows in RFP plasmas. In Sec. V, we examine the connection between the tearing mode rotation and plasma flow and directly test the commonly held assumption that the mode phase velocity is indicative of the plasma flow at the resonant surface. In Sec. VI, we evaluate different potential mechanisms for the momentum loss observed during PPCD and show why the drag from eddy currents in the conducting shell is the most important. Finally, in Sec. VII, we summarize our results and draw conclusions.

II. EXPERIMENTAL SETUP AND DIAGNOSTICS

MST is bounded by a conducting shell with a major radius of $R = 1.5$ m and a minor radius of $a = 0.52$ m. The experiments described in this paper were done at high plasma current, $I_p = 500$ kA, in deuterium. The well-developed Pulsed Parallel Current Drive (PPCD) technique was used to achieve periods of improved confinement.[30] During

PPCD, the inductive poloidal and toroidal electric fields at the plasma boundary are manipulated to drive additional current along the magnetic field in the edge. Figure 1(a) shows the toroidal magnetic flux which drops significantly when PPCD is applied from approximately 10 to 20 ms. After a brief transition period that can last a few milliseconds, the broad spectrum of tearing mode activity typical of standard RFP plasmas is reduced. Confinement improves as illustrated by the increase in soft x-ray (SXR) emission shown in Fig. 1(b). Brief interruptions in the improved confinement sometimes occur due to bursts of magnetic fluctuation activity, causing a sudden drop in the SXR emission. A small burst of this type occurs in the discharge shown around 13 ms. For our analysis, we consider only discharges with long burst-free periods and limit our analysis of flow and mode rotation to burst-free periods.

The largest of the tearing modes in PPCD discharges in MST is the $(m, n) = (1, 6)$ mode, and the toroidal phase velocity of this mode is often used as a proxy for toroidal plasma rotation in MST. This mode is resonant in the core (see Fig. 2) and hence is expected to have a phase velocity that is closely related to the plasma velocity in that region. The phase velocities of the magnetic modes are measured with a toroidal array of coils at the plasma boundary. Figure 1(c) shows that the $n = 6$ mode velocity has a complicated behavior prior to the onset of improved confinement but decays smoothly during the burst-free period. The rate of decay is not the same for all discharges. In some cases, the mode locks (no rotation in the lab frame) part way through PPCD while in other cases, like the one shown in the figure, rotation continues for the entire discharge. During the bursty MHD activity prior to PPCD onset or after PPCD has ended, it is common to see the mode velocity increase due to various intrinsic flow drive mechanisms that can be very large during periods of high fluctuations.[13,29] However, during the improved confinement period, we observe only decay of the mode rotation rate. The intrinsic flow drive seems to be weak or absent during the improved confinement period.
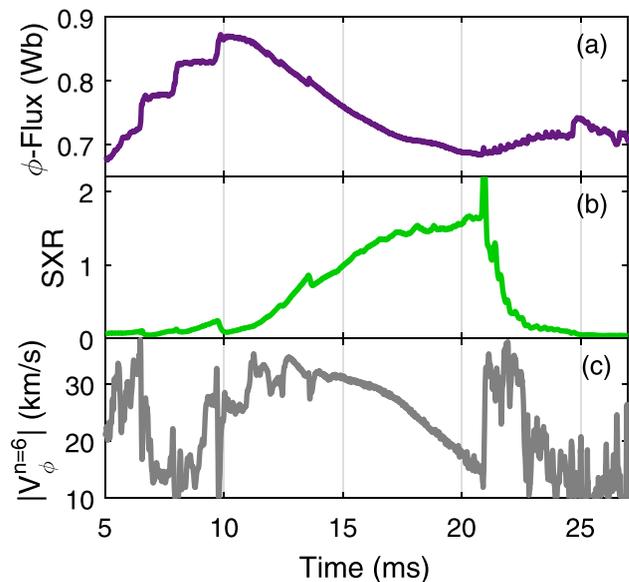

FIG. 1. (a) Toroidal magnetic flux, (b) soft X-ray emission (arbitrary units), and (c) $m = 1$, $n = 6$ toroidal phase velocity are shown for a typical PPCD discharge. PPCD is active from 10 ms to 20 ms.
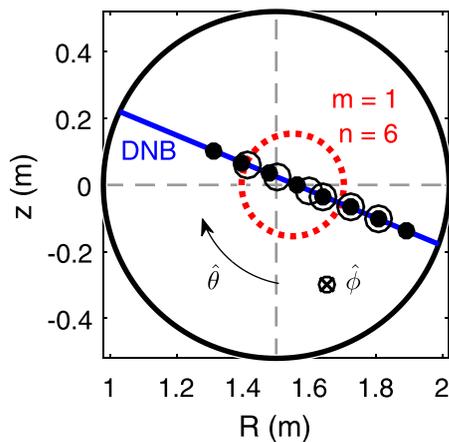
FIG. 2. A poloidal cross-sectional view of the MST with toroidal direction into the page and poloidal direction clockwise. Toroidal velocity measurement locations (open circles) and poloidal velocity measurement locations (solid circles) are shown along the path of the diagnostic neutral beam (blue line). The red dashed circle marks the location of the $(m, n) = (1, 6)$ tearing mode resonant surface.

All impurity ion velocity measurements in this paper were made with the CHERS diagnostic.[33,35,38] A 50 keV diagnostic neutral hydrogen beam stimulates charge exchange with C^{+6} ions. The resulting C^{+5} ions emit light that is Doppler shifted and Doppler broadened. The excited state lifetime is short enough ($\sim$1 ns) with respect to the ion gyrofrequency ($\sim$14 MHz) that the measured Doppler shift is representative of the impurity ion motion prior to charge exchange with the beam. We use the 343.4 nm C VI line corresponding to the C^{+5} $n = 7$–6 transition for the studies reported here. Our custom high-throughput spectrometer measures the emission with good time resolution (100 kHz) but at only one spatial location. Profiles of velocity are compiled by averaging the data from several similar shots and then moving the light collection fibers between shots. Photon counting noise is reduced, and measurement precision is improved by rebinning the data and fitting the line shape with a time cadence of 0.1 ms.

The beam is injected radially from the outboard side along a line that is tilted at an angle of 22.5° relative to the horizontal as shown in Fig. 2. The beam has low divergence and a minimum diameter of 3 cm at the point of best focus which corresponds roughly with the third solid circle from the outboard side in Fig. 2. The measurement volume for CHERS is limited to the intersection of the viewing chord and the beam. Poloidal viewing chords are situated perpendicular to the beam, and the emission is viewed from above. The measurement region for these chords extends about 1 cm in the radial direction and 3–5 cm in the poloidal and toroidal directions depending on the beam diameter at the viewing location in question. The solid circles in Fig. 2 show the locations where poloidal flow was measured. Beam attenuation and divergence reduce the signal level for the most inboard chords but good measurements were obtained at all of the locations shown in the figure.

The locations where toroidal flow measurements were made are shown by the open circles in Fig. 2. Toroidal viewing chords emanate from a single porthole displaced by a toroidal angle of 42° from the plane containing the beam and all poloidal viewing chords.[35] The toroidal viewing chord that intersects the beam on-axis is perpendicular to the beam while off-axis chords intersect the beam at angles that

are slightly less than 90°. Since radial flows are very small, specifically near the plasma axis, and the projection of any radial flow onto the line of sight is even smaller, all toroidal viewing chords measure predominantly toroidal flow. The radial extent of the measurement volume for these chords is about 2 cm. Mechanical limitations do not allow toroidal velocity measurements farther from the axis at present.

For this paper, we will define the positive toroidal direction to be into the page in Fig. 2 and the positive poloidal direction to be clockwise in the same figure. In these coordinates, the toroidal plasma current is negative and the equilibrium toroidal magnetic field in the core is positive for our discharges. The toroidal ion velocity and mode phase velocity in the core are in the same direction as the plasma current, and the poloidal ion velocity near the axis is in the clockwise direction. The current and flow parallel to the equilibrium magnetic field are such that $\mathbf{J} \cdot \mathbf{B} < 0$ and $\mathbf{v} \cdot \mathbf{B} < 0$ in the core for these plasmas.

III. ABSOLUTE VELOCITY CALIBRATION

Although the CHERS system has been operational on MST for many years, the accurate absolute wavelength calibration needed for velocity profile measurements was achieved only recently.[39] The spectrometer used for the CHERS measurement[33] records the C VI line shape as a function of time by measuring the intensity at 16 different wavelengths across a 0.06 nm interval centered on 343.4 nm. Absolute wavelength calibration requires either a light source with well-known wavelength in this narrow range or a plasma measurement where the velocity (and hence Doppler shift) is known to be zero. We developed a custom light source with a ultraviolet light emitting diode and etalon to provide a known calibration line in the region of interest. After calibration with this source, we confirmed that the Doppler shift of the charge exchange emission is in fact zero for the velocity measurement in the poloidal plane that coincides with the magnetic axis. (This location is the fourth solid circle from the left in Fig. 2.) The systematic uncertainty in the wavelength calibration is $\pm$0.003 nm which corresponds to a systematic uncertainty in velocity of $\pm$3 km/s.

One complication for CHERS measurements in MST is the existence of a large background signal. The background is due to a combination of O VI emission and C VI emission and is compensated for in every CHERS measurement using a slightly displaced viewing chord that passes just to the side of the neutral beam.[40] The background emission comes from a broad region throughout the plasma and is not suitable for absolute velocity calibration because the relative mixture of O VI and C VI is not well known and can change in time. During standard plasmas in MST, the contribution from O VI emission dominates due to the higher electron collisional excitation rate for O^{+5} relative to C^{+5}. In improved confinement PPCD discharges, the electron temperature increases substantially, and since O^{+5} ionizes more readily than C^{+5}, the O VI contribution to the background diminishes and C VI becomes dominant. The fine structure distortions to the line shape for O VI and C VI are slightly different; hence, when the relative strength of the lines varies, there is an apparent wavelength shift in the background emission even if the plasma is not moving. The shift results in an apparent change in velocity on the background view of up to 12 km/s if changes to the emission model are not taken into account in the fitting.

Fortunately, the charge exchange emission that is localized to the beam is dominated by C VI emission in all MST plasmas so uncertainty in the oxygen/carbon mix does not affect the interpretation of Doppler shifts from the active component of the emission. We have verified that

errors in the line shape model used to fit the passive background emission (e.g., errors caused by assuming O VI is dominant even when it is not) do not affect the compensation of the background in CHERS measurements. Hence, the inferred Doppler shift of the active charge exchange emission is robust to variations in the background emission model. The relative intensities of the charge exchange and background emissions do have a strong effect on the signal to noise ratio of the localized velocity measurement. Hence, the best absolute velocity calibration is obtained in high current PPCD plasmas where the background emission drops to a low value. Calibration using the measured wavelength of charge exchange emission from the magnetic axis during PPCD is simple to include in the run day and is now routinely performed.

Figure 3 shows an example discharge used for velocity calibration. The inferred velocity from the active charge exchange component is shown in panel (a), and the charge exchange and background emission intensities are shown in panel (b). Early in the discharge, the background emission is high and the charge exchange emission is relatively low. As PPCD progresses and confinement improves, the background emission drops and the charge exchange emission increases so that eventually they are comparable in amplitude. During this good confinement period, we set the measured velocity to zero. Typical uncertainties due to photon counting statistics are shown for three characteristic time points. Although the error bars overlap the zero velocity line at all times, the deviation from zero early in time illustrates the difficulty in achieving well-resolved velocity measurements when background emission is high. However, during the good confinement period, the calculated uncertainties from photon statistics, the observed scatter in the data itself from one time point to the next, and the systematic calibration errors are all consistent with an absolute velocity measurement that is trustworthy at the ± 3 km/s level.

IV. INTRINSIC ION FLOWS DURING IMPROVED CONFINEMENT

In this section, we describe the observed impurity ion velocity profiles and their time dependence in PPCD plasmas. The
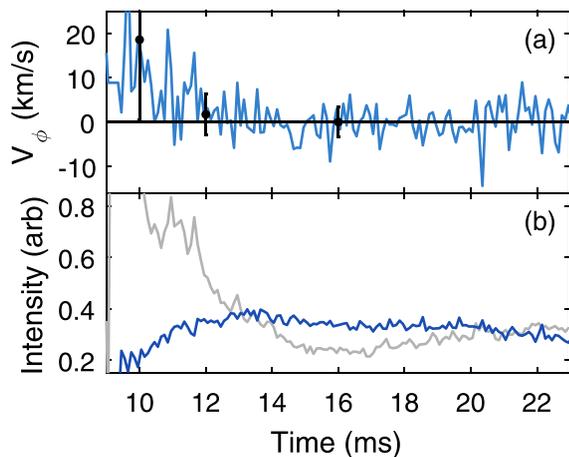
FIG. 3. Zero-flow calibration shot at $r = 0$ cm. (a) Calibrated poloidal velocity. The three error bars represent the measurement noise at three characteristic time points. (b) The intensities of the active charge exchange signal (dark blue) and the background signal (light gray) as functions of time.

measurement locations will be given in terms of the distance away from the point where the beam crosses the midplane. This point is within 1–2 cm of the magnetic axis in MSTFIT reconstructions[41] of the magnetic equilibrium; hence, the r values in these plots can be interpreted as flux surface radii.

A. Flow profile measurements with CHERS

The toroidal velocity profile [Fig. 4(a)] is peaked on the axis and has a relatively broad profile early in time. The profile early in PPCD is inherited from the intrinsic flow drive that acts prior to the transition to good confinement and suggests a broad forcing profile coupled with large momentum transport prior to PPCD. The flow exhibits inboard-outboard asymmetry with inboard toroidal flows being higher than outboard flows. The reason for this asymmetry is not known at present. As PPCD proceeds, the toroidal velocity decreases at off-axis locations but remains nearly constant near the axis. As a result, a strongly sheared flow profile develops. The rate at which the off-axis flow decreases is not the same for all discharges. Figure 4(a) shows the average behavior, taking into account shots that lock early in PPCD and those with only modest slowing down. The region where m = 1 tearing modes are resonant is shaded in the figure, and we note here that those are the areas where the flow appears to decrease in time. The m = 1, n = 6 resonant surface shown in Fig. 2 is at the inner boundary of this shaded region around r = 10–15 cm. There are no low order rational surfaces in the region near the axis where the toroidal flow persists during PPCD. We will return to this point later in the paper.
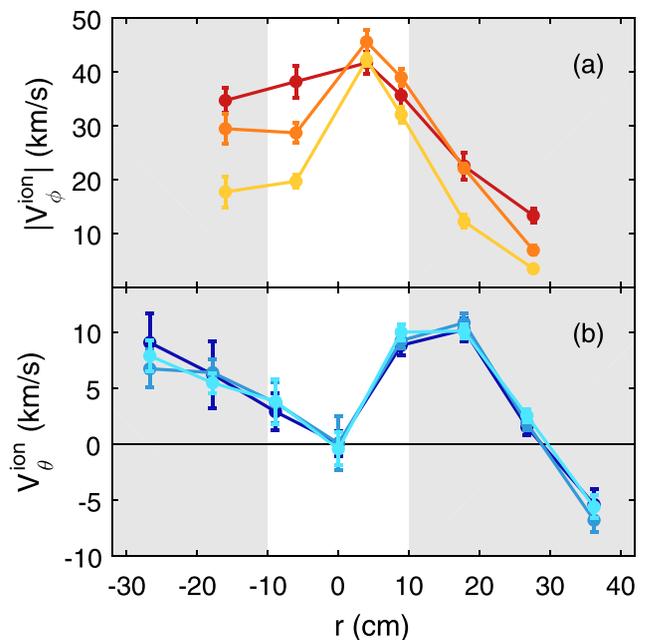
FIG. 4. (a) Toroidal and (b) poloidal flow profile evolution in time, averaged over several (4–9) shots for each location. Profile lines evolve from darkest to lightest tone, with time windows 12–14 ms, 15–17 ms, and 18–20 ms, respectively. Error bars represent the variation in the data from individual discharges. The shaded regions indicate the regions where tearing modes are resonant.

The poloidal velocity profile is shown in Fig. 4(b). The poloidal flows are weaker than the toroidal flows (note the difference in scale) and also exhibit the opposite form of inboard-outboard asymmetry. Outboard poloidal flows are stronger than inboard poloidal flows in the core. The poloidal flow on the outboard side reverses direction near the midradius but such a reversal is not observed on the inboard side within the radial extent of these measurements. It is possible that the flow does reverse at larger minor radius on the inboard side outside of our measurement area. Unlike the toroidal flow profile, the poloidal flow profile shows very little change in time during PPCD.

By combining poloidal and toroidal flow measurements from similar discharges, we can calculate the components of the flow parallel and perpendicular to the equilibrium magnetic field at each location

$$|v_\perp| = \frac{|v_\theta B_\phi - v_\phi B_\theta|}{B},\tag{1}$$

$$|v_\parallel| = \frac{|v_\theta B_\theta + v_\phi B_\phi|}{B}.\tag{2}$$

Here B, B_ϕ, and B_θ are obtained from MSTFIT reconstructions of the magnetic equilibrium constrained by total toroidal current, total toroidal flux, edge poloidal arrays of magnetic field coils, and 11-chord far infrared (FIR) polarimetery.[41] v_θ and v_ϕ are taken from Fig. 4 with v_θ positive and v_ϕ negative in our coordinate system. The resulting parallel and perpendicular flow profiles are shown in Fig. 5. While the flow is primarily along the magnetic field in the core, the two components become comparable at the midradius. The parallel flow profile
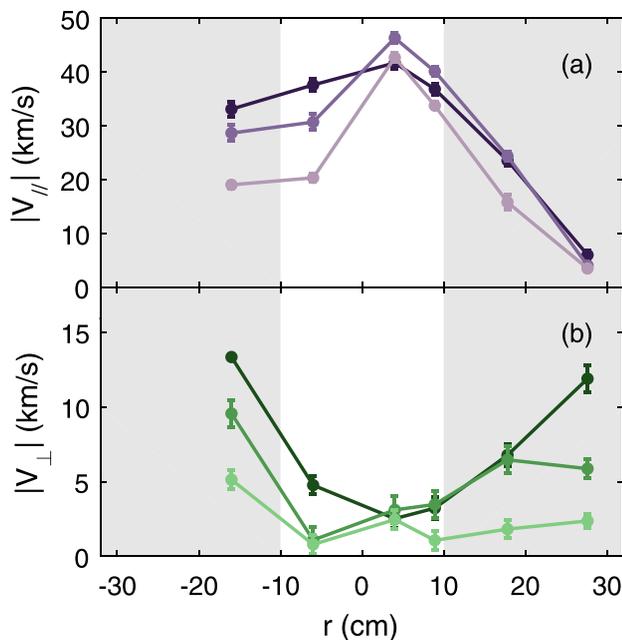

FIG. 5. (a) Parallel and (b) perpendicular flow profiles calculated from average poloidal and toroidal flows in Fig. 4. Profile lines evolve from darkest to lightest tone, with time windows 12–14 ms, 15–17 ms, and 18–20 ms. Error bars represent the variation in the data from individual discharges. The shaded regions indicate the regions where tearing modes are resonant.

decreases in time at off-axis locations, similar to the toroidal flow. Perpendicular flows decrease to nearly zero during PPCD. This likely reflects a decrease in the ambipolar radial electric field that is responding to reduced electron transport from magnetic stochasticity.

B. Comparison to previous measurements of flows in the RFP

Before moving on, we will briefly comment on how our measured flow profiles compare with past measurements in the RFP. Passive Doppler measurements of impurity ion flows in PPCD were made in the past at low plasma current (200 kA) in MST.[8] Different impurity ions were used to provide some degree of radial localization but the radial emission profile for all lines became hollow during PPCD. The toroidal flows measured in this way decreased with radius, consistent with the localized measurements presented here. The passive Doppler measurements indicated that the toroidal flow decreased in time although movement of the emission profiles during PPCD and lack of good radial resolution made it difficult to tell if the flow at a given radial point was actually decreasing. Our localized toroidal flow measurements show that the flow does indeed decrease in time at most radii. The persistent and strongly peaked flow in the core that we report here was not observed in the previous line-average measurements because of the lack of sensitivity in that region.

The parallel flow profile in the core of standard MST plasmas (not PPCD) was reported previously[13,29] and can be compared with our measurements early in PPCD before the onset of improved confinement. The previous measurements used Rutherford scattering[42] to obtain profiles of majority ion poloidal flows and used the rotation of the core-resonant m = 1 tearing modes to infer the toroidal flow. (We examine the validity of using mode phase velocities as a proxy for ion flows in Sec. V.) The parallel flow obtained in this way was in the cocurrent direction in the core (regardless of the sign of $J \cdot B$) and reversed sign near the midradius. Our parallel flow measurements early in PPCD [Fig. 5(a)] are also cocurrent in the core and decrease to near zero at the midradius on the outboard side. Our poloidal flow measurements reverse sign at r = +30 cm [Fig. 4(b)]. Unfortunately, geometrical limitations on the toroidal view do not allow us to make localized toroidal flow measurements at r > 28 cm. However, assuming that the toroidal flow remains near zero at r = +35 cm, the reversed sign of the poloidal flow implies $v \cdot B > 0$ at that point, consistent with the sign reversal reported earlier for standard plasmas. It is much less clear that the parallel flow reverses on the inboard side of the machine but we cannot rule that out with the data we have.

The pressure profile of the carbon ions is fairly flat in the core of MST plasmas;[36] hence, the diamagnetic flows are small. This implies that the direction of the perpendicular flow should be indicative of the $E \times B$ velocity due to the ambipolar radial electric field. Our measured perpendicular flows are in a direction consistent with a positive E_r in the core throughout PPCD. [The $v_\phi B_\theta$ term in Eq. (1) is larger than the $v_\theta B_\phi$ term for all of our measurement locations.] This is consistent with radial electric field measurements inside the reversal surface in a number of RFP devices[11] and is as expected for a plasma where the stochastic magnetic field in the core favors more rapid electron losses relative to ion losses. As noted earlier, the observed decay of the perpendicular flow in our PPCD plasmas is consistent with the decay of this ambipolar electric field as should occur with the reduction of magnetic stochasticity during PPCD. Heavy ion beam probe measurements of electric
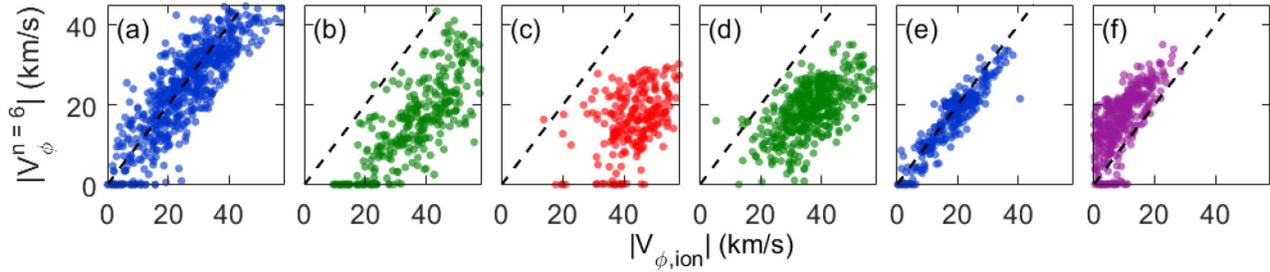
FIG. 6. Correlation between the $m = 1$, $n = 6$ mode phase velocity and toroidal ion flow for all shots and times at (a) $r = -16$ cm, (b) -6 cm, (c) $+4$ cm, (d) $+8.9$ cm, (e) $+17.8$ cm, and (f) $+26.7$ cm. The dotted line represents a 1:1 correlation.

potential in the core of similar PPCD plasmas show a decaying positive electric potential and hints of a decaying outward radial electric field as well.[43]

V. ION VELOCITY AND MODE ROTATION

The relatively quiet conditions during PPCD provide a good opportunity to compare the observed tearing mode rotation to the measured plasma flow. This provides a direct test of the no-slip assumption that the plasma and mode move together in the region around the mode resonant surface. The condition for mode resonance is $\boldsymbol{k} \cdot \boldsymbol{B} = 0$. If the mode and plasma move together, then the frequency of the mode in the lab frame will be $\omega = \boldsymbol{k} \cdot \boldsymbol{v}$. Since $\boldsymbol{k}$ is perpendicular to $\boldsymbol{B}$ at the resonant surface, one can see that ω only depends on $v_\perp$. Flows along $\boldsymbol{B}$ propagate through the magnetic island structure, not across it, and therefore purely parallel flows at the resonant surface should not produce any apparent motion of the mode in the lab frame. Combining the equation for resonance with the equation for mode frequency leads to an equation for the toroidal phase velocity of the mode, $v_{m,n}$, in terms of the plasma flows and equilibrium magnetic fields at the resonant surface

$$v_\phi^{m,n} = \frac{\omega}{k_\phi} = v_\phi - \frac{B_\phi}{B_\theta} v_\theta. \tag{3}$$

A key prediction of the no-slip theory is that the flows that matter are the ones at the resonant surface. Figure 6 shows the correlation between the measured phase velocity of the $m = 1$, $n = 6$ mode and the toroidal flow measured at different locations. The data include multiple shots and multiple time points within each shot. One can see that the ion flow and the mode velocity correlate well near the mode resonant surface (recall Fig. 2) but the correlate gradually gets worse as

the distance from the resonant surface increases. The toroidal flow near the magnetic axis [Fig. 6(c)] seems nearly independent of the mode velocity. The dashed lines in the figure indicate a 1:1 match between mode phase velocity and toroidal flow. It is interesting that the mode velocity matches the toroidal flow alone near the resonant surface. Locations inside of this lie to one side of the 1:1 line and locations outside lie to the other side. This is somewhat surprising given that Eq. (3) predicts that the poloidal flow should also play a role in determining the mode phase velocity.

Figure 7 shows the correlation between the measured phase velocity and the poloidal flow. As can be seen, the poloidal flow does not correlate well with variations in the mode velocity at any radius. Although we cannot measure toroidal and poloidal flow at the same time due to diagnostic limitations, it seems clear that the toroidal flow at the mode resonant surface is a better predictor of the mode phase velocity than the combination of toroidal and poloidal flows given in Eq. (3). Correlations with other mode numbers show similar results.

The close coupling between toroidal flow and mode velocity and the weak coupling between poloidal flow and mode velocity can also be seen in the time dependence of the flows on individual shots. Figure 8 illustrates this using two shots with very similar mode velocity evolution. The mode slows down rapidly in these shots, locking around 14 ms. The toroidal flow near the resonant surface [Fig. 8(a)] slows to a value consistent with zero, albeit with some delay relative to the mode. The delay may be related to viscous coupling between the plasma inside of the magnetic island and the surrounding plasma. Surprisingly, the poloidal flow near the resonant surface [Fig. 8(b)] remains nearly constant in time, consistent with the fixed poloidal flow profiles shown earlier.
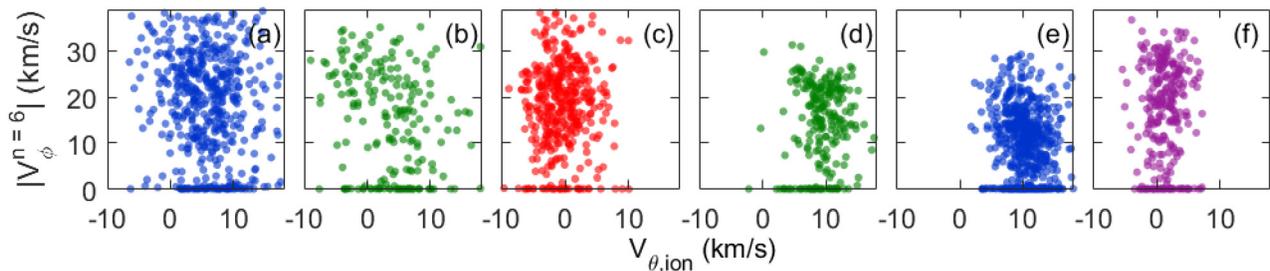

FIG. 7. Correlation between the $m = 1$, $n = 6$ mode velocity and poloidal ion flow for all shots and times at (a) $r = -17.8$ cm, (b) -8.9 cm, (c) 0 cm, (d) 8.9 cm, (e) 17.8 cm, and (f) 26.7 cm.
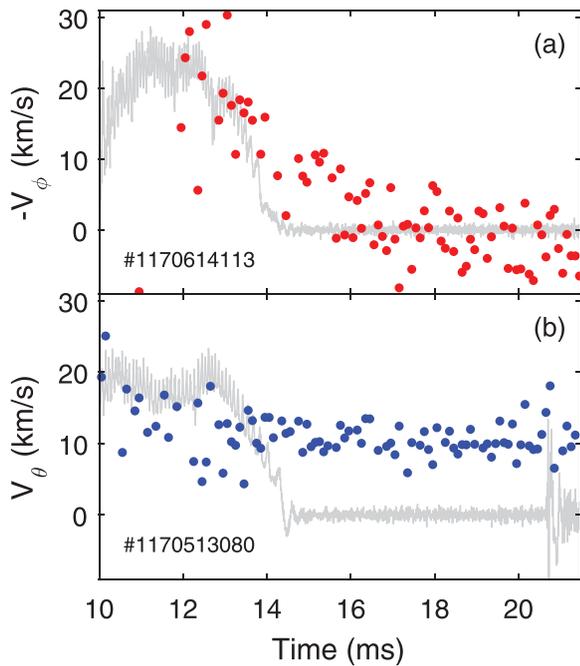
FIG. 8. Lines show the m = 1, n = 6 toroidal phase velocity for two similar shots [(a) and (b)]. Dots represent the measured ion flow near the resonant surface: (a) toroidal flow at r = −16 cm and (b) poloidal ion flow at r = +17.8 cm.

Early work on tearing mode rotation in tokamaks implied that the tearing mode islands corotate with the electron fluid[14] and hence Eq. (3) may not strictly apply if the carbon ion flow is used. However, later theoretical work showed that the modes could rotate with the ions or electrons depending on the size of the islands and other effects.[44,45] Experimental observations in the RFX reversed field pinch and DIII-D and JET tokamaks, for example, have confirmed that island propagation in the ion diamagnetic drift direction is common.[22,25,46] In our plasmas, as noted earlier, the carbon ion diamagnetic flow is very small in the core and the measured perpendicular flow of carbon ions decays away during PPCD. The electron and majority ion diamagnetic flows near the m = 1, n = 6 resonant surface are also expected to be fairly small in these plasmas. The smallness of all of these flows makes it difficult to say with certainty if the mode is comoving with the ions or electrons here. However, the correlation information and the rigidity of the poloidal flow seem to suggest that it is the toroidal plasma flow rather than the perpendicular plasma flow that better follows the mode rotation.

VI. MOMENTUM LOSS MECHANISM DURING PPCD

In Secs. IV and V, we have described the observations of flow profile evolution and the connection between the mode rotation and the flow. In this section, we investigate possible mechanisms for the slowing down during the good confinement period. For each mechanism, we perform a simple estimate of the time scale for slowing down for comparison with the experimentally observed time scale of 2–10 ms. We also look for correlation of the deceleration rate with observables that should be important for each proposed mechanism. Only the last of the mechanisms we describe satisfies both of these

tests, i.e., it has the right slowing down time scale and the right scaling with key observables. This mechanism is the electromagnetic torque caused by eddy currents in the aluminum shell that are induced by rotation of the dominant m = 1, n = 6 mode.

The first mechanism we examine is the drag caused by charge exchange between plasma ions and neutral particles.[2] The 2D neutral deuterium density profile has been modeled using plasma density measurements from FIR interferometry, line-integrated D_α emission on several chords, and the magnetic equilibrium provided by MSTFIT. A lower limit on the flow damping time is given by the inverse of the rate at which charge exchange reactions occur between ions and neutrals. This is a lower limit because it assumes that neutrals have no average flow and that neutral charge exchange products are promptly lost from the plasma. Both of these assumptions are probably false in MST but relaxing these would only make the damping time longer. The neutral density in the core of these plasmas is calculated to be $n_D \sim 1 \times 10^{14}\,m^{-3}$. The ion temperature is measured by CHERS to be $T_i \geq 400\,eV$ which implies the specific rate coefficient for charge exchange is $\langle \sigma v \rangle \sim 6 \times 10^{14}\,m^3/s$. Hence, the time for slowing down by neutral drag is

$$\tau_{neutral} \sim \frac{1}{n_D \langle \sigma v \rangle} \sim 170\ \text{ms.} \qquad (4)$$

This is much longer than the observed slowing down time.

Confirmation that neutral drag is not the primary slowing down mechanism is obtained by examining the correlation between the toroidal deceleration rate, $-\frac{dv}{dt}$, and the D_α intensity. We use a D_α viewing chord with the impact parameter of r/a = +0.3 as a typical example here. The average deceleration rate is calculated by fitting a straight line to the n = 6 mode velocity [see Fig. 1(c)] during the time of good confinement when the mode is continuously slowing down. Figure 9(a) shows that there is no observable correlation between the deceleration rate and the D_α intensity. This confirms the conclusion based on numerical estimates of the slowing down time. Neutral drag is not the dominant mechanism in these plasmas.

During standard RFP plasmas, momentum transport has been shown to be consistent with what is expected from the motion of plasma particles in the stochastic magnetic field produced by multiple overlapping tearing mode islands.[16,17,47] Momentum transport due to stochastic magnetic fields has also been shown to be an important process in stellarators.[48] In stochastic magnetic fields, the momentum diffusion coefficient is equal to the magnetic field line diffusivity multiplied by the sound speed. The slowing down time scale can be written as

$$\tau_{stochastic} = \frac{\Delta r^2}{L_c c_s} \left(\frac{B_0}{B_r} \right)^2, \qquad (5)$$

where $\Delta r \sim 0.4$ m is the distance from the n = 6 resonant surface to the wall, $L_c \sim 10$ m is the parallel correlation length, $c_s \sim 3 \times 10^5$ m/s is the sound speed, $B_0 \sim 0.5$ T is the equilibrium magnetic field strength, and δB_r is the radial magnetic field fluctuation amplitude in the stochastic region. The magnetic fluctuation amplitude in the core of these plasmas is $B_r \sim 2$ mT. Inserting this into Eq. (5) yields $\tau_{stochastic} \sim 3$ ms, on the order of the observed slowing down time. However, the mode spectrum is strongly peaked in these plasmas so that the total rms magnetic fluctuation amplitude is dominated by the n = 6 mode. One large mode does not lead to stochasticity in the field and
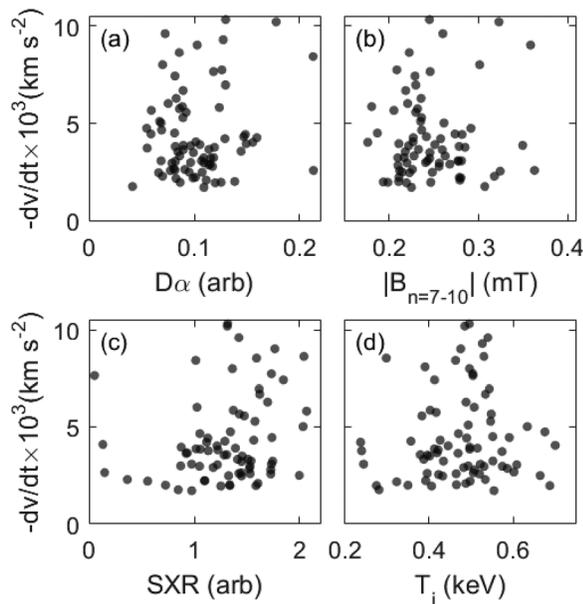
FIG. 9. Correlation between the (m, n) = (1,6) mode deceleration and (a) neutral deuterium intensity, (b) combined rms mode amplitude for n = 7–10, (c) average soft X-ray emission during 18–20 ms, and (d) ion temperature. D_α and SXR are uncalibrated. Each data point represents one shot.

hence the magnetic stochasticity may be better quantified by the amplitudes of the secondary n = 7–10 modes. The rms average of the secondary mode amplitudes is given by

$$|B_{n=7-10}| = \left(\sum_{n=7}^{10} B_n^2 \right)^{1/2}. \qquad (6)$$

Using the secondary modes rather than the dominant mode gives $B_r \sim 0.3$ mT. Using this in Eq. (5), we obtain $\tau_{stochastic} \sim 150$ ms which is much longer than the observed slowing down time.

If the momentum transport resulting from a stochastic magnetic field were an important mechanism, we would expect the deceleration rate to correlate with the level of magnetic stochasticity and with the sound speed which in turn depends on electron and ion temperature. The stochasticity is determined primarily by the amplitude of the secondary modes, n = 7–10. Figure 9(b) shows that there is no observable correlation between the slowing down rate and the rms amplitude of the secondary modes defined in Eq. (6). Figures 9(c) and 9(d) show the correlation with maximum soft x-ray intensity (which is typically higher when electron temperature is higher) and ion temperature measured with CHERS. If the deceleration rate scaled with the sound speed, there should be a correlation here but there is not. This lack of correlation with secondary modes, electron temperature, and ion temperature, coupled with the numerical estimates above, implies that the stochastic momentum transport is not the dominant slowing down mechanism for the plasma as a whole. However, the residual stochasticity could still play a role in providing enhanced momentum transport in the midradius region where the islands overlap.

The reduction in magnetic stochasticity during PPCD strongly affects electron energy confinement which in turn affects the maximum electron temperature attained during PPCD. The global energy confinement time in these plasmas has been studied previously[30] and is on the of order $\tau_E \sim 5$ ms, similar to the slowing down time. If momentum transport correlates with energy transport, then one might expect to see the slowing down time correlate with the maximum soft x-ray intensity which is a crude proxy for the quality of electron energy confinement improvement. As already noted, Fig. 9(c) shows that there is no observable correlation between these quantities. Hence, although the global energy confinement time is of similar magnitude to the slowing down time, it does not appear that better energy confinement necessarily correlates with weaker deceleration rates.

The classical[49] perpendicular ion viscosity is given by

$$\eta_\perp = \frac{3nkT_i}{10\omega_{ci}^2 \tau_i}, \qquad (7)$$

where ω_{ci} is the ion cyclotron frequency and τ_i is the ion-ion collision time. The ion collision time is sensitive to impurity densities and charge state populations which are not fully known in these plasmas. The collision time for D-D interactions is $\tau_{DD} \sim 2$ ms. Impurities could enhance the effective collisionality somewhat but probably not by more than one order of magnitude. The time to damp the core plasma rotation by classical viscous coupling with the wall is then

$$\tau_{vis} = \frac{m_i n a^2}{\eta_\perp}. \qquad (8)$$

Using the D-D collision time, this gives $\tau_{vis} \sim 40$ s so that even if impurities are included, the time is far too long to explain the observed deceleration. In addition, if classical viscosity is important, it is expected that the deceleration rate would correlate with the ion temperature but Fig. 9(d) shows that it does not. Furthermore, the behavior of the toroidal flow profile in time strongly suggests that the drag mechanism operates primarily near the mode resonant surfaces, and there is no reason to expect that the classical viscosity has this kind of radial structure.

One mechanism does seem promising as an explanation for the observed deceleration, namely, the electromagnetic torque resulting from eddy currents generated in the aluminum shell by the rotating magnetic fluctuations.[20] This has been shown to be important during quasisingle helicity (QSH) discharges in MST where the dominant mode grows to large amplitude.[21] The strong mode growth observed in QSH plasmas does not occur in most of the discharges studied here but the eddy current mechanism can still be important, specifically if the intrinsic flow drive that normally operates in standard plasmas has been reduced or eliminated in PPCD. The eddy-current torque acts in the vicinity of the mode resonant surfaces and hence can explain the observed profile evolution including the lack of significant flow damping near the magnetic axis. The magnitude of the torque due to the n = 6 mode has been estimated to be on the order of $T_{em} \sim 1$ Nm in these plasmas using Eq. (36) in Ref. 21. If this torque is applied to an isolated toroidal shell of plasma with a thickness of ~ 0.1 m located at the n = 6 resonant surface, we would observe a deceleration time of $\tau_{em} \sim 1$ ms. Factoring in the interaction of this plasma shell with the
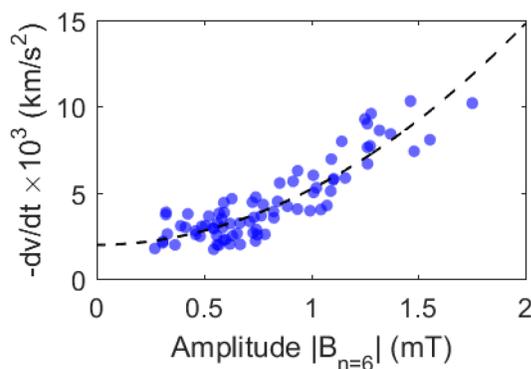
FIG. 10. Correlation between the $n = 6$ mode deceleration and $n = 6$ mode amplitude. A quadratic model gives the best fit.

surrounding plasma, a deceleration time of a few milliseconds is reasonable and on the order of what is observed.

If the eddy current explanation is correct, we expect there to be an approximately quadratic dependence of the deceleration rate on the dominant $n = 6$ mode amplitude. This is because the torque on the plasma results from a $\mathbf{j} \times \mathbf{B}$ force acting near the resonant surface. Figure 10 shows that there is indeed a strong correlation between the deceleration rate and the mode amplitude. The data are consistent with a quadratic dependence as shown by the fitted curve. The finite deceleration implied by the fit at zero mode amplitude may indicate the residual slowing down caused by other mode numbers. Taken together with the other evidence, this quadratic dependence strongly supports the conclusion that the eddy current drag is the dominant mechanism for the decay of the toroidal rotation observed in these plasmas.

VII. CONCLUSION

We have described the first localized flow profile measurements by charge exchange recombination spectroscopy (CHERS) in a reversed field pinch. The new capability is a direct result of recent improvements in absolute wavelength calibration that are robust and relatively simple to implement on a daily basis. We have applied the new capability to improved confinement plasmas that make use of the PPCD technique for magnetic fluctuation reduction. The measurements show that the ion flow in MST is primarily parallel to the mean magnetic field in the core and is peaked on the axis. As PPCD proceeds and the plasma confinement improves, the toroidal flow in much of the plasma gradually slows, coincident with the slowing of the dominant tearing mode rotation and consistent with the lack of substantial intrinsic flow drive. A small region near the magnetic axis does not slow down, resulting in the development of a strongly sheared flow profile near the axis.

We have directly examined the connection between tearing mode rotation and ion flows in these discharges and find that the mode rotation is strongly correlated with the ion flow at the resonant surface and weakly correlated with the flow away from the resonant surface. The mode rotation is much better correlated with the toroidal flow than with the poloidal flow which is largely unaffected during the slowing down of the modes and toroidal flow. We evaluated neutral

particle drag, momentum transport due to magnetic stochasticity, and classical viscosity, and found that none of them are good candidates for explaining the observed loss of momentum during PPCD. Instead, the best explanation is a drag on the plasma produced by eddy currents in the conducting shell associated with the rotation of the dominant tearing mode. Residual magnetic stochasticity may play a secondary role in distributing this momentum loss to the plasma around other nearby resonant surfaces.

Theoretical work on intrinsic flow drive in the RFP context is not highly developed and would be helpful for making a bridge between what is observed in the RFP and other devices like tokamaks and stellarators. For example, it seems experimentally that the kinetic stress is the likely source of momentum in the core of standard RFP plasmas.[29] It is not clear, however, exactly how this stress arises, how it scales with plasma and machine parameters, and in what other situations outside of the RFP it may be important. The theory is much better developed for the interaction of the tearing modes with the plasma flow and with the conducting shell. Although there are some differences, much of the physics that applies to mode rotation in the RFP also applies to tokamaks and similar devices. For example, the eddy current drag that appears to dominate here in PPCD plasmas is a common momentum loss mechanism in other plasmas with a conducting shell. More detailed modeling of mode and plasma flow behavior in PPCD may help to refine these models.

Computational studies of intrinsic flow drive and momentum transport in the RFP are also quite limited. A few recent single and two-fluid simulations of RFP plasmas have moved somewhat in this direction by examining the Maxwell and Reynolds stresses due to tearing fluctuations and the subsequent effects on the momentum density profile.[19,50,51] With the reduction in fluctuations during PPCD, these stresses are greatly reduced and possibly insignificant. However, prior to PPCD onset, these stresses can be strong and they combine with other intrinsic flow drivers (like the kinetic stress) to set the initial flow profile heading into PPCD. In two-fluid simulations with no initial flows,[19] a sheared parallel momentum profile is produced during periods of strong fluctuation activity. The direction of the resulting parallel flow in the core of the simulations is in the countercurrent direction, inconsistent with the parallel flows reported here and elsewhere for RFP experiments. Hence, as the authors of that study note, the Maxwell and Reynolds stresses caused by the tearing modes flatten the parallel momentum profile during periods of high fluctuation activity but they are not responsible for driving the peaked parallel momentum profiles observed in the experiment.

In the future, it would be interesting to apply the localized flow measurements to standard RFP plasmas and try to gain additional insight into the radial profile and scaling of the intrinsic flows with magnetic fluctuation level. It would also be interesting to develop a better understanding of the inboard-outboard asymmetries in the flows and the reasons why the poloidal flow profile appears to be so rigid in time in these plasmas while the toroidal flow is not. The strong connection between tearing mode velocity and plasma flow has already been exploited in several devices to control plasma rotation and to do perturbative experiments that enable studies of momentum transport.[17,52] It would be interesting to see to what degree this could be used with active multimode feedback to shape the flow profile and open new avenues for controlling transport.

ACKNOWLEDGMENTS

REFERENCES

[1] K. Ida and J. E. Rice, Nucl. Fusion **54**, 045001 (2014).
[2] J. E. Rice, Plasma Phys. Controlled Fusion **58**, 083001 (2016).
[3] P. Diamond, Y. Kosuga, Ö. Gürcan, C. McDevitt, T. Hahm, N. Fedorczak, J. Rice, W. Wang, S. Ku, J. Kwon, G. Dif-Pradalier, J. Abiteboul, L. Wang, W. Ko, Y. Shi, K. Ida, W. Solomon, H. Jhang, S. Kim, S. Yi, S. Ko, Y. Sarazin, R. Singh, and C. Chang, Nucl. Fusion **53**, 104019 (2013).
[4] H. Arimoto, K. Sato, A. Nagata, S. Masamune, Y. Aso, K. Ogawa, S. Yamada, A. Matsuoka, H. Oshiyama, and T. Tamaru, Nucl. Fusion **27**, 1021 (1987).
[5] D. J. Den Hartog, A. F. Almagri, J. T. Chapman, H. Ji, S. C. Prager, J. S. Sarff, R. J. Fonck, and C. C. Hegna, Phys. Plasmas **2**, 2281 (1995).
[6] L. Carraro, M. E. Puiatti, F. Sattin, P. Scarin, and M. Valisa, Plasma Phys. Controlled Fusion **40**, 1021 (1998).
[7] H. Sakakita, Y. Yagi, Y. Hirano, and S. Sekine, J. Phys. Soc. Jpn. **69**, 635 (2000).
[8] H. Sakakita, D. Craig, J. K. Anderson, T. M. Biewer, S. D. Terry, B. E. Chapman, D. J. Den-Hartog, and S. C. Prager, Jpn. J. Appl. Phys., Part 2 **42**, L505 (2003).
[9] F. Bonomo, D. Bonfiglio, P. Piovesan, L. Piron, B. Zaniol, S. Cappello, L. Carraro, R. Cavazzana, M. Gobbin, L. Marrelli, E. Martines, B. Momo, M. E. Puiatti, and M. Valisa, Nucl. Fusion **51**, 123007 (2011).
[10] V. Antoni, D. Desideri, E. Martines, G. Serianni, and L. Tramontin, Nucl. Fusion **36**, 1561 (1996).
[11] V. Antoni, D. Desideri, E. Martines, G. Serianni, and L. Tramontin, Phys. Rev. Lett. **79**, 4814 (1997).
[12] V. Antoni, H. Bergsåker, G. Serianni, M. Spolaore, N. Vianello, R. Cavazzana, G. Regnoli, E. Spada, E. Martines, M. Bagatin, and J. R. Drake, J. Nucl. Mater. **313–316**, 972 (2003).
[13] A. Kuritsyn, G. Fiksel, A. F. Almagri, D. L. Brower, W. X. Ding, M. C. Miller, V. V. Mirnov, S. C. Prager, and J. S. Sarff, Phys. Plasmas **16**, 055903 (2009).
[14] G. Vahala, L. Vahala, J. H. Harris, G. Bateman, and B. V. Waddellt, Nucl. Fusion **20**, 17 (1980).
[15] R. Howell, J. Ingraham, G. Wurden, P. Weber, and C. Buchenauer, Phys. Fluids **30**, 1828 (1987).
[16] A. F. Almagri, J. T. Chapman, C. S. Chiang, D. Craig, D. J. Den Hartog, C. C. Hegna, and S. C. Prager, Phys. Plasmas **5**, 3982 (1998).
[17] R. Fridström, B. E. Chapman, A. F. Almagri, L. Frassinetti, P. R. Brunsell, T. Nishizawa, and J. S. Sarff, Phys. Rev. Lett. **120**, 225002 (2018).
[18] A. K. Hansen, A. F. Almagri, D. Craig, D. J. D. Hartog, C. C. Hegna, S. C. Prager, and J. S. Sarff, Phys. Rev. Lett. **85**, 3408 (2000).
[19] J. P. Sauppe and C. R. Sovinec, Phys. Plasmas **24**, 056107 (2017).
[20] R. Fitzpatrick, S. Guo, D. J. Den Hartog, and C. C. Hegna, Phys. Plasmas **6**, 3878 (1999).
[21] B. E. Chapman, R. Fitzpatrick, D. Craig, P. Martin, and G. Spizzo, Phys. Plasmas **11**, 2156 (2004).
[22] D. Terranova, T. Bolzonella, and S. C. Guo, Plasma Phys. Controlled Fusion **47**, 1047 (2005).
[23] Y. Yagi, H. Koguchi, H. Sakakita, S. Sekine, Y. Maejima, J. A. B. Nilsson, T. Bolzonella, and P. Zanca, Phys. Plasmas **6**, 3824 (1999).
[24] P. Zanca, E. Martines, T. Bolzonella, S. Cappello, S. C. Guo, P. Martin, S. Martini, S. Ortolani, R. Paccagnella, D. Terranova, and M. Viterbo, Phys. Plasmas **8**, 516 (2001).
[25] R. J. La Haye, C. C. Petty, E. J. Strait, F. L. Waelbroeck, and H. R. Wilson, Phys. Plasmas **10**, 3644 (2003).
[26] L. Piron, D. Bonfiglio, P. Piovesan, B. Zaniol, F. Auriemma, L. Carraro, L. Chacón, L. Marrelli, M. Valisa, M. Veranda, and M. Zuin, Nucl. Fusion **53**, 113022 (2013).
[27] M. Okabayashi, P. Zanca, E. J. Strait, A. M. Garofalo, J. M. Hanson, Y. In, R. J. La Haye, L. Marrelli, P. Martin, R. Paccagnella, C. Paz-Soldan, P. Piovesan, C. Piron, L. Piron, D. Shiraki, and F. A. Volpe, Nucl. Fusion **57**, 016035 (2017).
[28] R. Dexter, D. Kerst, T. Lovell, S. Prager, and J. Sprott, Fusion Technol. **19**, 131 (1991).
[29] W. X. Ding, L. Lin, D. L. Brower, A. F. Almagri, B. E. Chapman, G. Fiksel, D. J. Den Hartog, and J. S. Sarff, Phys. Rev. Lett. **110**, 065008 (2013).
[30] B. E. Chapman, A. F. Almagri, J. K. Anderson, T. M. Biewer, P. K. Chattopadhyay, C. S. Chiang, D. Craig, D. J. Den Hartog, G. Fiksel, C. B. Forest, A. K. Hansen, D. Holly, N. E. Lanier, R. O'Connell, S. C. Prager, J. C. Reardon, J. S. Sarff, M. D. Wyman, D. L. Brower, W. X. Ding, Y. Jiang, S. D. Terry, P. Franz, L. Marrelli, and P. Martin, Phys. Plasmas **9**, 2061 (2002).
[31] T. Nishizawa, A. F. Almagri, J. K. Anderson, W. Goodman, M. J. Pueschel, M. D. Nornberg, S. Ohshima, J. S. Sarff, P. W. Terry, and Z. R. Williams, Phys. Rev. Lett. **122**, 105001 (2019).
[32] G. F. Abdrashitov, V. I. Davydenko, P. P. Deichuli, D. J. Den Hartog, G. Fiksel, A. A. Ivanov, S. A. Korepanov, S. V. Murakhtin, and G. I. Shulzhenko, Rev. Sci. Instrum. **72**, 594 (2001).
[33] D. Craig, D. J. Den Hartog, D. A. Ennis, S. Gangadhara, and D. Holly, Rev. Sci. Instrum. **78**, 013103 (2007).
[34] S. Gangadhara, D. Craig, D. Ennis, D. Hartog, G. Fiksel, and S. Prager, Phys. Rev. Lett. **98**, 075001 (2007).
[35] R. M. Magee, D. J. Den Hartog, G. Fiksel, S. T. A. Kumar, and D. Craig, Rev. Sci. Instrum. **81**, 10D716 (2010).
[36] S. T. A. Kumar, D. J. Den Hartog, V. V. Mirnov, K. J. Caspary, R. M. Magee, D. L. Brower, B. E. Chapman, D. Craig, W. X. Ding, S. Eilerman, G. Fiksel, L. Lin, M. Nornberg, E. Parke, J. A. Reusch, and J. S. Sarff, Phys. Plasmas **19**, 056121 (2012).
[37] D. A. Ennis, D. Craig, S. Gangadhara, J. K. Anderson, D. J. Den Hartog, F. Ebrahimi, G. Fiksel, and S. C. Prager, Phys. Plasmas **17**, 082102 (2010).
[38] D. Craig, D. J. Den Hartog, G. Fiksel, V. I. Davydenko, and A. A. Ivanov, Rev. Sci. Instrum. **72**, 1008 (2001).
[39] M. M. Baltzer, D. Craig, D. J. Den Hartog, T. Nishizawa, and M. D. Nornberg, Rev. Sci. Instrum. **87**, 11E509 (2016).
[40] S. Gangadhara, D. Craig, D. A. Ennis, and D. J. Den Hartog, Rev. Sci. Instrum. **77**, 10F109 (2006).
[41] J. K. Anderson, C. B. Forest, T. M. Biewer, J. S. Sarff, and J. C. Wright, Nucl. Fusion **44**, 162 (2004).
[42] J. C. Reardon, G. Fiksel, C. B. Forest, A. F. Abdrashitov, V. I. Davydenko, A. A. Ivanov, S. A. Korepanov, S. V. Murachtin, and G. I. Shulzhenko, Rev. Sci. Instrum. **72**, 598 (2001).
[43] D. R. Demers, X. Chen, P. M. Schoch, and P. J. Fimognari, Rev. Sci. Instrum. **81**, 10E109 (2010).
[44] R. Fitzpatrick and F. L. Waelbroeck, Phys. Plasmas **15**, 012502 (2008).
[45] R. Fitzpatrick and F. L. Waelbroeck, Phys. Plasmas **16**, 072507 (2009).
[46] P. Buratti, E. Alessi, M. Baruzzo, A. Casolari, E. Giovannozzi, C. Giroud, N. Hawkes, S. Menmuir, and G. Pucella, Nucl. Fusion **56**, 076004 (2016).
[47] J. M. Finn, P. N. Guzdar, and A. A. Cherniko, Phys. Fluids B **4**, 1152 (1992).
[48] K. Ida, M. Yoshinuma, H. Tsuchiya, T. Kobayashi, C. Suzuki, M. Yokoyama, A. Shimizu, K. Nagaoka, S. Inagaki, K. Itoh, T. Akiyama, M. Emoto, T. Evans, A. Dinklage, K. Du, K. Fujii, M. Goto, T. Goto, M. Hasuo, C. Hidalgo, K. Ichiguchi, A. Ishizawa, M. Jakubowski, K. Kamiya, H. Kasahara, K. Kawamura, D. Kato, M. Kobayashi, S. Morita, K. Mukai, I. Murakami, S. Murakami, Y. Narushima, M. Nunami, S. Ohdach, N. Ohno, M. Osakabe, N. Pablant, S. Sakakibara, T. Seki, T. Shimozuma, M. Shoji, S. Sudo, K. Tanaka, T. Tokuzawa, Y. Todo, H. Wang, H. Yamada, Y. Takeiri, T. Mutoh, T. Imagawa, T. Mito, Y. Nagayama, K. Y. Watanabe, N. Ashikawa, H. Chikaraishi, A. Ejiri, M. Furukawa, T. Fujita, S. Hamaguchi, H. Igami, M. Isobe, S. Masuzaki, T. Morisaki, G. Motojima, K. Nagasaki, H. Nakano, Y. Oya, Y. Suzuki, R. Sakamoto, M. Sakamoto, A. Sanpei, H. Takahashi, M. Tokitani, Y. Ueda, Y. Yoshimura, S. Yamamoto, K. Nishimura, H. Sugama, T. Yamamoto, H. Idei, A. Isayama, S. Kitajima, S. Masamune, K. Shinohara, P. S. Bawankar, E. Bernard, M. Von Berkel, H. Funaba, X. L. Huang, T. Ii, T. Ido, K. Ikeda, S. Kamio, R.

Kumazawa, C. Moon, S. Muto, J. Miyazawa, T. Ming, Y. Nakamura, S. Nishimura, K. Ogawa, T. Ozaki, T. Oishi, M. Ohno, S. Pandya, R. Seki, R. Sano, K. Saito, H. Sakaue, Y. Takemura, K. Tsumori, N. Tamura, H. Tanaka, K. Toi, B. Wieland, I. Yamada, R. Yasuhara, H. Zhang, O. Kaneko, and A. Komori, Nat. Commun. **6**, 5816 (2015).

[49]S. I. Braginskii, Rev. Plasma Phys. **1**, 205 (1965).

[50]F. Ebrahimi, V. V. Mirnov, and S. C. Prager, Phys. Plasmas **15**, 055701 (2008).

[51]J. P. Sauppe and C. R. Sovinec, Phys. Plasmas **23**, 032303 (2016).

[52]P. Piovesan, D. Bonfiglio, F. Auriemma, F. Bonomo, L. Carraro, R. Cavazzana, G. De Masi, A. Fassina, P. Franz, M. Gobbin, L. Marrelli, P. Martin, E. Martines, B. Momo, L. Piron, M. Valisa, M. Veranda, N. Vianello, B. Zaniol, M. Agostini, M. Baruzzo, T. Bolzonella, A. Canton, S. Cappello, L. Chacón, G. Ciaccio, D. F. Escande, P. Innocente, R. Lorenzini, R. Paccagnella, M. E. Puiatti, P. Scarin, A. Soppelsa, G. Spizzo, M. Spolaore, D. Terranova, P. Zanca, L. Zanotto, and M. Zuin, Phys. Plasmas **20**, 056112 (2013).